Building and Environment 211 (2022) 108743

Contents lists available at ScienceDirect

Building and Environment

journal homepage: www.elsevier.com/locate/buildenv

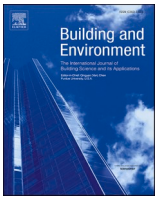

Self-cleaning durability assessment of TiO_2/SiO_2 photocatalysts coated concrete: Effect of indoor and outdoor conditions on the photocatalytic activity

Souad Khannyra [a,b], Manuel Luna [a], M.L. Almoraima Gil [a,*], Mohammed Addou [b], Maria J. Mosquera [a,**]

[a] TEP-243 Nanomaterials Group, Department of Physical-chemistry, Faculty of Sciences, University of Cadiz, 11510, Puerto Real, Spain
[b] Materials and Valorization of Natural Resource Laboratory, FST Tangier, Abdelmalek Essaadi University, Morocco

ARTICLE INFO

Keywords:
Concrete
Self-cleaning
NOx
TiO_2 /SiO_2 photocatalyst
Durability

ABSTRACT

A self-cleaning nanostructured TiO_2 coating has demonstrated the capacity to mitigate undesired effects from air pollution. Not only it reduces the deterioration of building materials but may also prevent certain pollution-related human health problems. In this study, mesoporous TiO_2/SiO_2 photocatalysts were synthesized in order to produce self-cleaning and long-lasting coatings that meet the necessary requirements for outdoor applications. The synthesized products were sprayed on concrete substrates and their self-cleaning and air depolluting capabilities were evaluated. The former one as a function of methylene blue (MB) and soot degradation and the latter, according to nitrogen oxides reduction. The coatings proved to have high photocatalytic activity, and their efficiency was enhanced as TiO_2 loadings were increased. Thus, after the first 60 min of their irradiation by UV–vis light, the photocatalysts ST1 and S4T had removed 79% and 95% of the MB, respectively. These coatings presented particulate surfaces that provided more surface area and porosity, which are key factors for a high photocatalytic activity. Moreover, the same samples after 104 h of irradiation exhibited 38% and 49% conversion of total NO, respectively. While E503, a commercially available photocatalyst, produced coating cracked surfaces and a total MB degradation of just 50% after 60 min of irradiation as well as 35% of NO conversion after 104 h of irradiation. The TiO_2/SiO_2 coatings' photocatalytic efficacy remained practically invariable after four months of exposure to real-life conditions and three MB degradation cycles. After the outdoor durability tests, the coated surfaces exhibited a practically unchanged structure, which confirms their long-lasting efficiency.

1. Introduction

Increasing pollution, particularly in urban areas, has recently triggered the interest of many researchers towards the preservation of building materials. Concrete-based buildings are often exposed to a wide variety of pollutants, such as the particulate matter (PM) that is mainly associated to vehicle emissions as well as other inorganic pollutants like nitrogen oxides. According to recent statistics, more than 3000 kilotons of PM and 7000 tons of NOx are emitted every year just in Europe [1]. These pollutants not only affect the aesthetic and structure of certain building materials but also represent a public health concern. It has actually been demonstrated that NOx can be the cause of cancer as well as of other health threatening conditions [2]. In addition, the particulate matter released by vehicles and industrial facilities is mainly constituted by soot [3], which not only ends up depositing on building facades and negatively affect their appearance [4], but also may be the cause of certain respiratory and cardiovascular diseases [5]. A well-known study, *An Association between Air Pollution and Mortality in Six U.S. Cities*, which was started in 1973 and used data from 14 to 16 years, demonstrated the significant correlation between particulate pollution and mortality increments due to cardiopulmonary diseases. In fact, a considerable number of studies have focused on this topic and investigated on the different options to reduce pollution in urban areas. Among the different effective solutions used for both the preservation of building materials and the reduction of air pollution, massive depolluting surfaces based on photocatalysis seem to be a promising approach [6–9]. Semiconductors

* Corresponding author.
** Corresponding author.
E-mail addresses: almoraima.gil@uca.es (M.L.A. Gil), mariajesus.mosquera@uca.es (M.J. Mosquera).

https://doi.org/10.1016/j.buildenv.2021.108743
Received 14 September 2021; Received in revised form 10 December 2021; Accepted 29 December 2021
Available online 4 January 2022

have been widely studied and received noteworthy attention in recent years because of their immense photoactivity as well as optical, and electrical features. From the moment when TiO_2 photoactivity was discovered [10], it was considered as a most suitable photocatalyst because of its stability, ready availability, low cost, lack of toxicity and a high photocatalytic efficiency [11–19]. Besides the photochemical properties exhibited by TiO_2 when activated by UV light, when TiO_2 is exposed to ultraviolet radiation a photoinduced phenomenon takes place [20,21]. This is known as super-hydrophilicity, which consists on a reduction of water contact angle that results in a uniform water film covering the treated surfaces [22,23]. This water film prevents any contact between the external dirt and the actual covered surface.

TiO_2 has been currently used in a wide range of applications such as glass [24], textiles [25] or air purification [26]. Hence, by applying a TiO_2 photocatalyst coating on concrete surfaces, building facades might be efficiently protected, while at the same time, air pollution would be reduced.

A number of studies have investigated the use of self-cleaning building materials based on their photocatalytic activity [27–30]. In fact, some research works have already confirmed how effective TiO_2 NPs can be regarding the oxidation of NOx as well as other organic pollutants when subjected to solar irradiation [31–33]. Zouzelka et al. demonstrated that the concentration of both NO and NO_2 in the air could be significantly reduced as an effect of photocatalytic processes [34]. Another study reported the high efficiency levels reached by TiO_2 when used to remove dye staining and to reduce air pollution, with almost total RhB molar conversions and over 53% NOx photo oxidation [35]. Ballari et al. determined the efficiency of concrete paving stones containing TiO_2 for the oxidation of nitrogen oxides (NO_x). According to their results, under UV irradiation, these materials would reach NO_x abatement levels between 20% and 30% [36].

Applying a TiO_2 photocatalyst on building's facades for its self-cleaning properties, and air depolluting capabilities under solar radiation seems to be a rather interesting tactic. However, the use of this type of photocatalyst for outdoor applications would require the employment of an appropriate matrix to ensure an excellent durability and adherence onto the buildings' facades. In this order of things, silica has been considered as a potentially suitable matrix for the immobilization of TiO_2 on building surfaces. Over recent years, numerous studies have investigated the capacity of siloxanes to create durable and well-adhere coatings that successfully immobilize TiO_2 on building facades [37–40].

Nevertheless, the number of research studies that can be found until present on the durability of self-cleaning coatings on building materials under real-life conditions is rather limited. Thus, a considerable number of studies have focused on the durability of TiO_2 photocatalyst coatings. Different methods have been employed to determine self-cleaning durability under indoor or outdoor conditions. Graziani et al., for instance, investigated the durability of self-cleaning TiO_2 coatings on fired clay brick facades where the photocatalytic activity was determined before and after the ageing test. Their results revealed that the photocatalytic efficiency of TiO_2 remains stable after the ageing process, which confirms TiO_2 good photocatalytic efficiency when applied to clay brick substrates [20]. Pinho et al. developed a sol containing silica oligomer and titanium particles and sprayed it on friable building materials. The resulting nanomaterial produced effective adhesive and crack-free layers on the stone surface and provided it with self-cleaning properties [41]. Rosales et al. conducted a number of adhesion tests to evaluate the durability of SiO_2, TiO_2, or TiO_2–SiO_2 coatings on mortar surfaces. The photocatalytic measurements revealed that the efficiency of TiO_2 had decreased, while no difference could be observed with regard to the efficacy of SiO_2 and TiO_2–SiO_2. These results revealed that by adding silica to TiO_2 its durability would improve without impairing its photocatalytic activity [42].

Several commercial products containing TiO_2 NPs, such as E503 from Nanocer, are available on the market. However, once its solvents evaporate, even though a certain coating is produced, it does not adhere well to building surfaces. Pinho et al. evaluated the performance of two commercial products: E503 and TV100. After characterizing the coatings, it was revealed that they present a cracked surface and a low mechanical resistance when applied on stone.

In the present work, a number of synthesized TiO_2/SiO_2 sols have been applied onto concrete substrates and assessed for MB and soot degradation as well as for NOx oxidation. Let us mention that this work has a dual objective: firstly, to determine the penetration depth of the photocatalytic sols into the substrate structure as well as the self-cleaning ability of the coatings; secondly, to determine the self-cleaning durability of the coatings both under indoor and outdoor conditions. Specifically, to determine the durability of the self-cleaning properties of the coatings under indoor conditions, each one of the substrates covered with one of the different coatings in the study was subjected to MB degradation cycles in triplicate so that long-term degradation could be assessed. Regarding the outdoor test, the samples were exposed to real-life conditions for four months, and their surfaces were verified by SEM in order to determine any relation between their topographic structure and their photocatalytic performance efficiency. Self-cleaning durability, in these cases, was also determined according to MB photodegradation.

2. Materials and methods

2.1. Synthesis of the different photocatalysts and their application

The commercially available TiO_2 known as VP Aeroperl 25/20 (produced by Evonik, Essen, Germany), which consists in a 20 μm average particle size microgranulate and 50 ± 15 m^2 surface area, was mixed with the silica precursor TES40 WN (Wacker, Munich, Germany) and with an ethoxysilane (average degree of polymerization 5) oligomer that provides approximately 41% of the silica upon complete hydrolysis. The mixture was sonicated for 20 min in an ultrasonic bath and then water and n-octylamine (Sigma-Aldrich, St. Louis, Missouri, United States) were added and the mixture was agitated under high-power ultrasound at 120 W for 10 min by means of a Bandelin Sonopuls HD3200 ultrasonic homogenizer (Berlin, Germany). The amount of water and n-octylamine with respect to the silica oligomer were 0.83% v/v and 0.36% v/v, respectively. The TiO_2 proportions employed were 0,1, and 4% (w/v) with respect to the silica oligomer. The formulations tested have been designated as follows: S0T, S1T and S4T (where the numbers refer to the concentration percentages of TiO_2).

For further comparison, the commercial photocatalytic E503 manufactured by Nanocer was also applied on concrete substrates, this product consists in a TiO_2 water-based sol containing 7500 to 10,000 ppm of the oxide.

The products were sprayed onto concrete surfaces until saturation, the surfaces were kept wet for 1 min and then the sol excess was removed by means of a compressed air jet. Thereafter, the samples were weighed to determine the uptake of the products and dried under laboratory conditions for over a month period.

The substrates employed in this study were made of HERPLAC® concrete, consisting in a homogeneous structure on a fibreglass reinforced concrete (GFRC) board composed by 0.1–6 mm particle size dolomitic and limestone aggregates and white Portland cement CEM I 52.5R. The substrates were vibro-compacted and armed using alkali resistant fibreglass, manufactured by HERMESA STONE, S.L. The water/cement ratio and the cement/sand ratio (w/w) employed for this preparation were 1:2 and 1:5, respectively. This concrete presents a homogeneous structure and has an open porosity of 12.15 ± 1% calculated according to a European Standard [43]. The whiteness of this concrete makes of it an ideal material to evaluate surface staining.

2.2. Characterization

Immediately after the sols were synthesized, their rheological

properties were determined using a concentric cylinder viscometer (model DV-II+ with UL/Y adapter) by Brookfield (Middleborough, Massachusetts, United States). The experiments were performed at constant 25 °C by continuous recirculation of the water from a thermostatic bath. Shear stress versus shear rate flow curves were obtained.

The xerogels under study were obtained by depositing 20 ml of the sols in plastic 85 mm diameter Petri dishes and kept at room temperature (18 ± 0.5 °C relative temperature and 50 ± 3% humidity). The spontaneous sol-gel transition took place overnight, and the gels were dried under laboratory conditions until constant weight was reached. The resulting xerogels were characterised as follows:

Their UV–visible reflectance spectra were recorded by means of a UV-2600 spectrophotometer manufactured by Shimadzu and equipped with an ISR-2600 integrating sphere. $BaSO_4$ powder was used as the reference.

The powdered xerogels were characterized by means of a JEOL 2010F TEM/STEM microscope operating at 200 kV. This equipment has a spatial resolution of 0.19 nm on High Resolution Transmission Electron Microscopy (HRTEM) mode. The High Angle Annular Dark Field Scanning Transmission Electron Microscopy (HAADF-STEM) images were recorded using an 0.5 nm electron probe and 10 cm camera length. The powdered xerogel was deposited onto lacey carbon coated copper grids.

For further investigation, certain textural parameters such as pore size distribution and surface area were calculated as a function of N_2 physisorption at 77 K as determined by means of a Quantachrome Autosorb IQ. The adsorption data were determined following the NLDFT (Non-Local Density Functional Theory) approach [44], which allows to quantify both micro and mesoporous content and to determine pore size distribution when materials exhibit pores of different geometries.

The hydrodynamic sizes of the particles in the synthesized sols and their Z potentials were measured by means of a Zetasizer Nano ZS analyser manufactured by Malvern Instruments, which is based on Dynamic Light Scattering (DLS). The sols were diluted at 1/10 in ethanol.

2.3. Performance and durability evaluation

The colour change induced by the application of the sols was evaluated by means of a solid reflection spectrophotometer Colorflex manufactured by HunterLab. The conditions used were: illuminant D65 and observer 10°. CIELa*b* colour space and variations in colour were evaluated based on total colour difference (ΔE*) [45].

The topography of the concrete surfaces was visualized by Scanning Electron Microscopy (SEM), using a FEI Nova NanoSEM 450 microscope. The secondary electron images were acquired at 5 kV acceleration voltage and high vacuum conditions using a Through the Lens Detector (TLD). The samples were previously sputtered with a 9 nm gold coating to prevent electrical charging.

An Atomic Force Microscopy (AM-AFM, Nanotec Electrónica S.L.) operating in tapping mode was used to observe the topography of the surfaces under study. The Root Mean Square (RMS) roughness values were calculated based on 2.5 μm × 2.5 μm images.

A number of peeling tests using Scotch® MagicTM tape (3 M) were conducted to determine the adhesion of the coating onto the concrete surfaces [46]. The tests were performed by sticking a section of the adhesive tape onto the desired surface and then measuring the tape weight increment after detaching it from the surface.

The standard procedure was modified so that it could be used to determine the self-cleaning activity of the samples [47]. Firstly, 0.5 mM of the methylene blue (MB) solution was prepared in ethanol, and then this solution was deposited on the surface of the treated samples as well as on their untreated counterparts. The amount of solution to be used was determined by the surface area to be stained at 20 μl/cm^2. Then, the samples were irradiated inside a Solarbox 3000eRH solar degradation chamber manufactured by CO.FO.ME.GRA. and equipped with a 2500 W xenon arc lamp as well as an outdoor UV filter. Temperature, humidity, and irradiance (in the range of 300–800 nm) were monitored and controlled. The conditions in the chamber were 300 W/m^2 irradiance, 55 °C temperature and 60 mg/m^3 absolute humidity. The evolution of the diffuse reflection spectra was monitored over the irradiation time by means of the previously described solid spectrophotometer. The Kubelka-Munk function was used to determine equivalent absorbance and MB degradation [48].

The self-cleaning effectiveness of the treated samples was assessed using soot, since it is a real contaminant of building facades in urban areas. Firstly, a commercial black carbon pigment (Printex U from Evonik) was dispersed in chloroform, at a concentration of 0.8 g/l, then 20 μl/cm^2 of this dispersion were deposited on the surface of the treated concrete samples and their untreated counterparts. Then, the stained samples were kept in absence of light for 30 min to allow them to reach equilibrium. They were then irradiated inside the solar degradation chamber under the same conditions employed for the photocatalytic degradation test of MB. The evolution of the diffuse reflection spectra was measured, and soot degradation was determined according to absorbance in the range 420–440 nm [49].

The air depolluting efficiency of the treated samples was also determined based on NO oxidation. The 8x8x2 cm^3 samples were employed to evaluate their NO oxidation ability according to a previously designed protocol [49].

The photoinduced hydrophilic behaviour of the treated samples was determined as a function of the water contact angle as measured by means of a software controlled contact angle analyzer Dataphysics Instruments OCA 15 plus. The measurements were carried out on samples that had been stored in the absence of light four days by depositing 5 μl water droplets on each sample's surfaces. Each sample measurement was replicated a minimum of 10 times. Then, the samples were irradiated for 3 h inside the solar degradation chamber (300 W, 60 °C, RH 60%) and their contact angle was measured again.

Finally, the self-cleaning durability of the treated samples was evaluated by following two different methods. Firstly, for indoor conditions, where the durability was evaluated through MB degradation, the test was run in triplicate on each sample type to determine self-cleaning durability under light irradiation. Secondly, for outdoor conditions, the samples were placed at a location that was largely exposed to a wide range of pollutants (Seville city centre) such as NOx, PM, and other organic and inorganic contaminants released by vehicles and industrial facilities. The samples remained outdoor for four months, from May 2018 until August 2018. The annual average of pollutants for 2018 was 26 μg/m^3, 16 μg/m^3, 22 μg/m^3, and 70 μg/m^3, for PM_{10}, $PM_{2.5}$, NO_2, and O_3, respectively, according to reports [50]. The solar irradiation during this period was between 18 °C and 43 °C. After the exposure period was completed, the samples were brought back into the laboratory and washed off using a pressured air jet and water. Then their self-cleaning durability was determined based on MB degradation. For a better insight on the effect of real-life conditions on the coatings morphology, the samples' surface topography was characterized by SEM microscopy.

3. Results and discussion

3.1. Sol-gel characterization

The rheological properties of synthesized sols are a key factor with respect to the penetration of the photocatalysts into the substrates. The viscosity of the prepared sols was determined immediately after they were synthesized. Table 1 summarizes the sols' viscosity values. The sols exhibited a Newtonian behaviour in the evaluated shear range. The viscosity values were calculated as the slope of the shear stress versus the shear rate curves. In all the cases, the linear regression coefficients were above 0.99. The obtained results demonstrated that the viscosity of S1T was slightly higher than that corresponding to S0T. The highest viscosity value corresponded to S4T, which was explained by the increment in

Table 1
Viscosity, Z potential and hydrodynamic size values of the prepared sols and textural properties of the obtained xerogels.

Sample	Viscosity (mPas)	Z potential	Size(d. nm)	S_{SA} BET (m^2/g)	Total pore volume (cm^3/g)
S0T	5.52	−21,9	9.5 ± 0.1	497	0.532
S1T	5.87	−17,7	151.4 ± 2.8	467	0.562
S4T	9.10	−14,4	200.6 ± 4.1	389	0.502

TiO_2 loading [51]. It can be clearly seen that in all the cases, the synthesized products exhibited a viscosity value below 10 mPas, which allows the sols' penetration into the porous substrate structure and favours the adhesion of the coating onto the surface. E503 showed a substantially lower viscosity value (0.282 mPas) because of the nature of this product, which consists in nanoparticles dispersed in certain solvents.

The particle size distribution and Z-potential of the synthesized sols were also evaluated using Dynamic Light Scattering (DLS). The obtained results are presented in Table 1 and Fig. S2 in the Supplementary Material. In the absence of TiO_2 the measured particle size was 9.5 nm, which corresponds to the initial silica particles produced during the sol synthesis. The particles sizes were considerably greater (151 and 201 nm) in the sols containing TiO_2. This could be attributed to the presence of TiO_2 agglomerates or to TiO_2 particles acting as silica nucleation centres that generate TiO_2–SiO_2 aggregates. On the other hand, the sols' zeta potential presented less negative values as the TiO_2 content in the sols was augmented. Such increase should be associated to the natural positive charge of TiO_2 particles [52]. Zeta potential values under −20 may promote particle agglomeration, which would explain the larger hydrodynamic size registered by S4T sols.

Regarding the UV–Vis absorption spectra (Fig. S1 in the Supplementary Material), the powdered xerogels from S1T and S4T showed a characteristic absorption of TiO_2 located within the UV region. The intensity of the absorption increased as TiO_2 content was raised.

The photocatalysts under study were characterized by TEM in order to gain further insight regarding particle size and their distribution inside the silica matrices. The obtained TEM images and their corresponding EDS mapping are presented in Fig. 1. All the composites presented two distinct domains that correspond to amorphous silica and

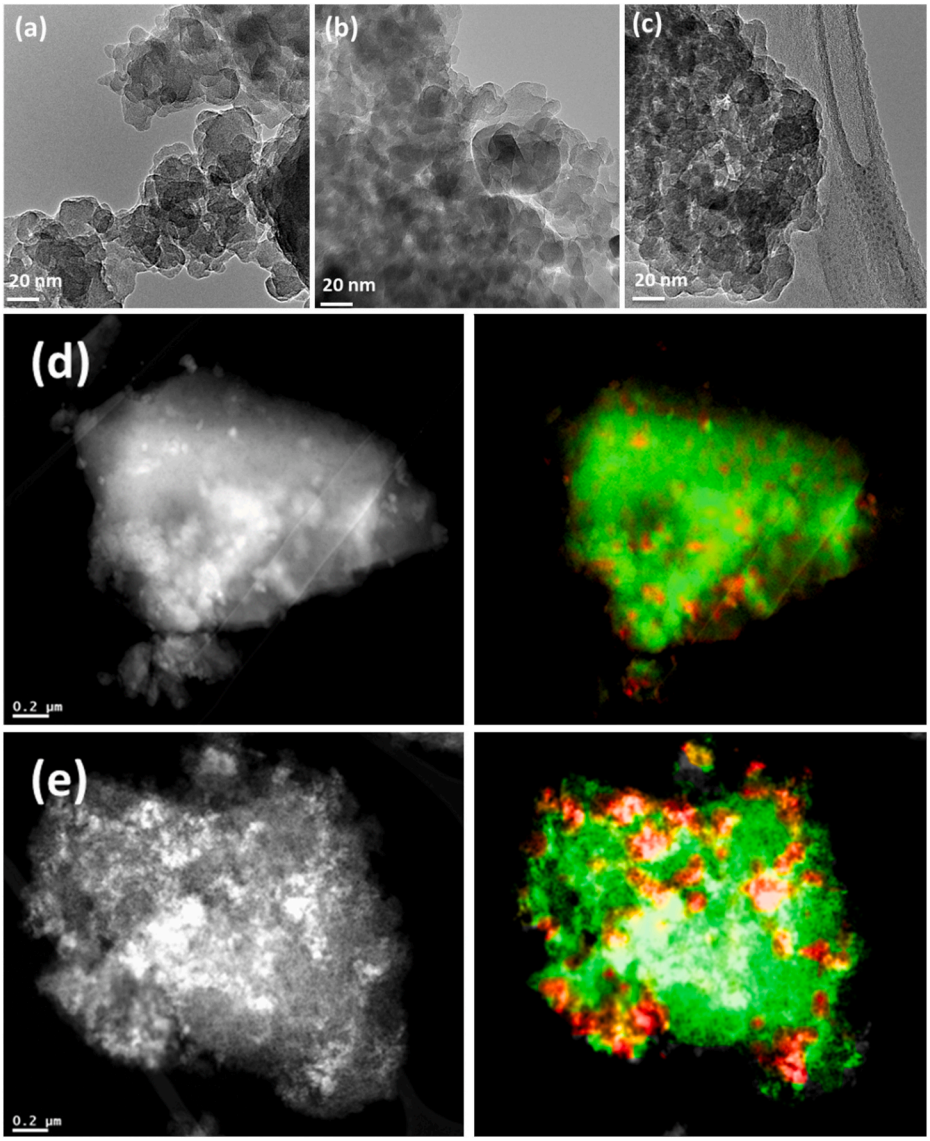

Fig. 1. HRTEM images of photocatalysts, S0T (a), S1T (b), S4T (c); and STEM-HAADF images with their corresponding Si (green) and Ti (red), S1T (d) and S4T (e) XEDS maps. (For interpretation of the references to colour in this figure legend, the reader is referred to the Web version of this article.)

to crystalline titanium NPs. Amorphous SiO_2 NPs are found in the form of aggregates with a size ranging between 10 and 25 nm. In all the composites, the silica NPs were found in the same size range, and no significant differences were observed. These results reflect those reported by Luna et al. for TiO_2/SiO_2 composites [53]. Regarding the photocatalysts behaviour of TiO_2 NPs, it was homogeneously distributed inside the silica matrices, which was confirmed by STEM-HAADF images in conjunction with XEDS mapping (Fig. 1; d and e). It could be clearly seen that TiO_2 NPs were well dispersed into the silica matrices in the form of aggregates under 100 nm size (Fig. 1d). This size would increase as TiO_2 loading was also increased and would reach an average size of about 200 nm in the case of S4T sols. This increment in agglomerations could be explained by the lower Z-potential value observed in S4T sols.

In order to further investigate the textural properties of the powdered xerogels, N_2 physisorption tests were conducted. The resulting adsorption–desorption isotherms and pore size distributions corresponding to the adsorption branches can be seen in Fig. 2, and their corresponding textural data are presented in Table 1. All the xerogels exhibited type IV(a) isotherms, which is a typical characteristic of mesoporous materials [54]. The hysteresis loops indicated an intermediate scenario between H_1 and H_2 with nearly parallel long branches that were neither vertical nor presented any triangular shapes [55]. Both types of hysteresis can be normally found in porous silica with ink-bottle pores, but H_2 is associated to complex pore-blocking structures, which makes us think that the developed materials may have a pore structure that presents a certain degree of blocking. Regarding the pore size distribution in these materials, the samples showed similar porosity distribution in the mesoporous range below 2 nm and in the mesoporous range ≈ 2–28 nm, with a maximum diameter between 3 and 8 nm. These pore sizes fit well with the interstitial spaces that are produced by the packing of the silica nanoparticles as observed by TEM. When the pore distributions of S0T and S1T are compared, it can be observed that S1T showed a greater fraction of over 7 nm size pores. This could be related to the addition of TiO_2 to the xerogel structure, being the size of TiO_2 particles greater than silica ones. On the contrary, the higher proportion of TiO_2 in S4T resulted in an evident reduction of the 8 nm size pore fraction. These changes in the structure of the xerogels are responsible for the differences that could be observed in their textural properties (see Table 1).

3.2. Assessment on concrete samples and comparison against commercial products

The products that had been synthesized for this study were sprayed on concrete substrates under laboratory conditions. Immediately after the sols were applied, the samples were weighed in order to calculate each product uptake. Table 2 shows the different product uptakes into the treated substrates. From the obtained results, it can be seen that there were no significant differences between the samples, with practically similar uptake values. A clear relationship between uptake and viscosity values (see Table 1) can be observed, except in the case of S4T sol, which presented similar uptake values regardless of the viscosity of the product (slightly higher viscosity than the other sols).

Table 2
Uptakes, total colour differences (ΔE*), peeling test results, contact angle values and NO removal of the treated samples and their untreated counterparts.

Samples	Uptake (mg/cm^2)	ΔE*	Amount of material removed by peeling (mg/cm^2)	Water contact angle (°)		% NO conversion
				Before	After	
Untreated	–	–	0.06	–	–	25
S0T	22.86 ± 1.91	1.44 ± 0.20	0.00	19.6 ± 3.5	19.4 ± 3.4	–
S1T	24 ± 1.88	1.32 ± 0.42	0.00	17.6 ± 3.9	16.7 ± 2.6	38
S4T	23.86 ± 1.67	0.97 ± 0.07	0.00	16.1 ± 3.6	9.3 ± 1.1	49
E503	24.16 ± 0.93	0.26 ± 0.11	0.19	–	–	35

In some cases, building material treatments may lead to undesired changes in surface appearance. This is a relevant aspect for applications where the aesthetical features of the building are to be preserved, and is particularly important in the case of cultural heritage buildings, where a total colour difference (ΔE*) of 3 is generally accepted as the maximum admissible threshold [56]. The obtained ΔE* values for the treatments developed in this work are included in Table 2. The results clearly indicated that the total colour change was rather similar in all the treatments, exhibiting a ΔE* value lower than 2 in all the cases, which would render this treatment suitable for application even in the most restrictive scenarios. Additionally, a slight decrease of ΔE* could be observed as TiO_2 content was increased, which is explained by the similar white colour of TiO_2 NPs and the substrates.

The SEM images of the samples' surfaces under study are shown in Fig. 3. All the treatments produced homogeneous coatings that thoroughly covered the original substrate surface. The only all-silica coating (S0T) presented a uniform, compact structure with the roughness corresponding to the silica particles that conform the xerogel. This is consistent with an earlier study by Pinho et al. [57]. On the other hand, the coatings containing TiO_2 presented structures that corresponded to the agglomeration of the particles, whose size matched P25 NPs. The size of the agglomerations slightly increased with TiO_2 loadings. We could, therefore, conclude that the silica sols penetrated in the porous substrate structures, while the TiO_2 NPs bonded by the silica would produce coatings with particulate surfaces comparable to those

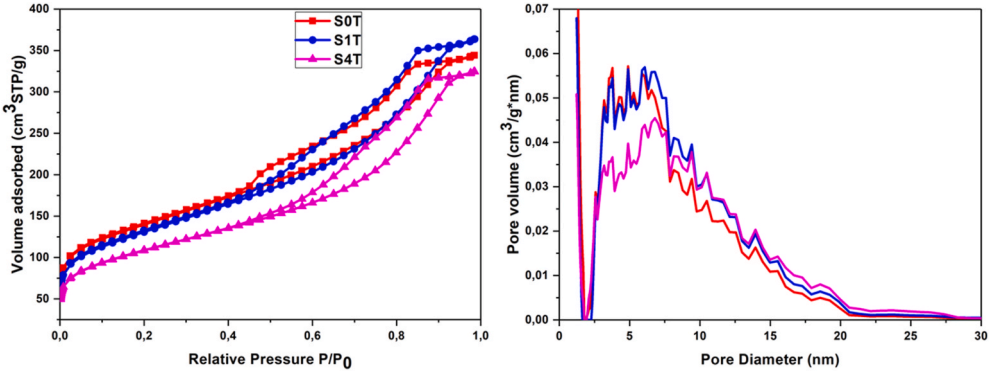

Fig. 2. Isotherms and NLDFT pore size distributions of the photocatalysts under study.

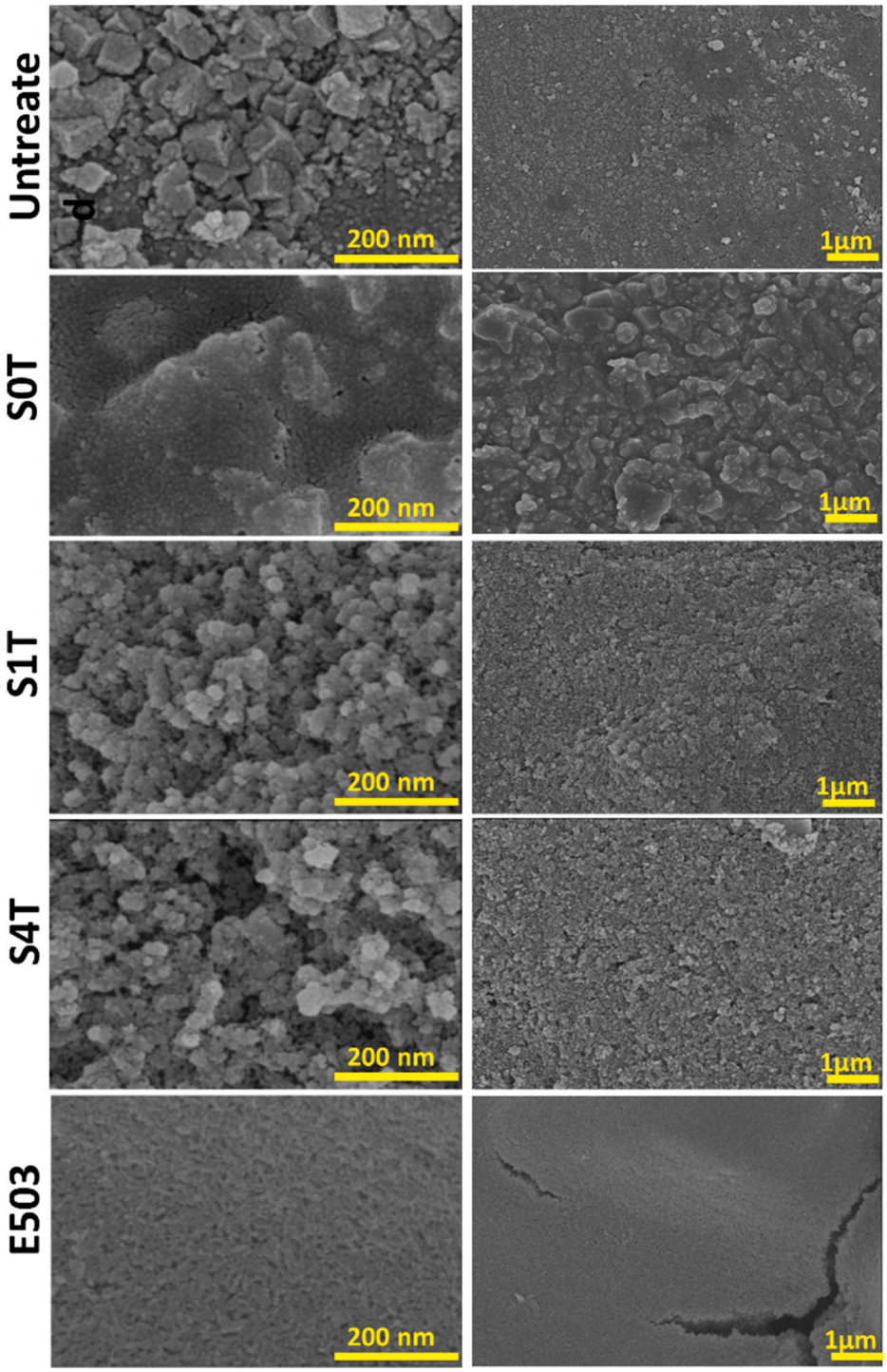

Fig. 3. SEM images of the untreated concrete surface and its treated counterparts at two different magnifications.

produced by the commercial product E503, which creates nano-structured coatings constituted by very small particles, that result in a smoother surface than that of the untreated samples (see Fig. S3 in the Supplementary Materials). A particulate surface has a higher surface area and porosity; therefore, an elevated photocatalytic activity can be generated. It is important to note that the developed products produced crack-free coatings, which confirms the positive behaviour of n-octylamine [29]. On the contrary, the commercial product E503 generated a nanostructured coating with a cracked surface.

The topography of the coatings surfaces in this study and that of their untreated counterparts were visualized by AFM. Fig. S3 displays the different 3D surface topographic images. The aggregate morphology presented by all the specimens are in agreement with the findings revealed by the SEM images. As already observed from the 3D surface plots, the untreated sample exhibited a higher roughness value (RMS = 127.58) compared to that of their treated counterparts S0T (RMS = 18.58), S1T (RMS = 30.93), S4T (RMS = 36.15) and E503(RMS = 75.80), this notable decrease in roughness values has been attributed to the presence of the coatings, that covers the intergranular space in the concrete substrates. Moreover, the coatings that contained TiO_2 NPs were significantly rougher than those containing just SiO_2, this roughness increment can be attributed to the size of the aggregates, which

becomes bigger as the amount of added TiO_2 is increased. With regard to the surfaces treated with E503, their roughness at 75.80 was also lower than that of the untreated sample, although it continued to be slightly higher than the roughness values measured from the samples treated with our sols. This roughness could be attributed to a poor adhesion of the product nanoparticles onto the intergranular spaces of the substrate or to the cracks that could be seen through SEM on the coating upper layers.

In order to better understand the actual penetration of the sols into the concrete substrates, MB-stained cross sections of the samples were examined (Fig. 4). MB allows to detect the presence of the sols inside the substrate and to determine how they have been absorbed. Thus, regular staining was observed in the untreated samples, whereas the treated samples were more intensely stained near the surface, indicating the presence of the sols. Penetration depth varied according to the features of the sprayed product (i.e., hydrophobic, hydrophilic). Thus, hydrophilic products spread over the surface of the substrate, increased contact area and prevented penetration. The deepest penetration was obtained by sample S0T, which is explained by the hydrophobic behaviour exhibited by the ethoxy groups in the sols before hydrolysis [29]. Consequently, as TiO_2 NPs are loaded, such hydrophobicity decreases, which results in a shallower penetration of the product. As the amount of TiO_2 added to the photocatalysts is increased, hydrophobicity tends to decrease due to the hydrophilic character of TiO_2 NPs [51] and poorer penetrations are achieved. Moreover, penetration depth also depends on sols viscosity, so that as viscosity increases, penetration depth decreases. These results are in agreement with viscosity values (see Table 1) and explain why the commercial product E503, with a lower viscosity (0.282 mPas), has demonstrated a slightly greater penetration than our synthesized products.

The samples' cross sections were also observed by SEM in order to confirm treatment penetration. Fig. 5 displays the SEM images of the untreated, E503 and S4T samples and their corresponding XEDS maps. This magnification allowed to examine each sample structure as well as Si, Ca and Ti distribution. Thus, Ca was the main element found, since this concrete is made of dolomitic and limestone aggregates. The aggregates of a bigger size could be easily identified as the grains where the Ca signal was more intense. Si was predominant in some grains and correspond to the silicate mineral impuritities that could be found in the aggregates. These two types of grains were embedded in a matrix where Si and Ca coexisted. The matrix was formed by hydrated cement paste and the thin aggregates. The elemental composition of this matrix at different depths was analysed in order to determine the penetration of the treatment product into the sample. Only on the surface of the substrate could Ti be found at its greatest concentration. On the other hand, Si could be found throughout the examined section of the treated samples, at concentrations that doubled those corresponding to the untreated substrate. These results indicate that the silica sol penetrated into the substrate while TiO_2 NPs remained on the surface. These findings are consistent with those previously commented with respect to roughness and that can be seen in Fig. 3.

In order to highlight the foregoing findings, a closer look at the S4T sample cross section (Fig. 6) should confirm the previous hypothesis on the product penetration. The sample's surface exhibited a thin layer that mainly consists in Si and Ti, which corroborates that the treatment produced a TiO_2/SiO_2 coating on the concrete surface. The coating layer is clearly visible in Fig. 6c, and its average thickness was 3 μm. After a closer examination of the coating composition (Fig. 6 area 1), it could be

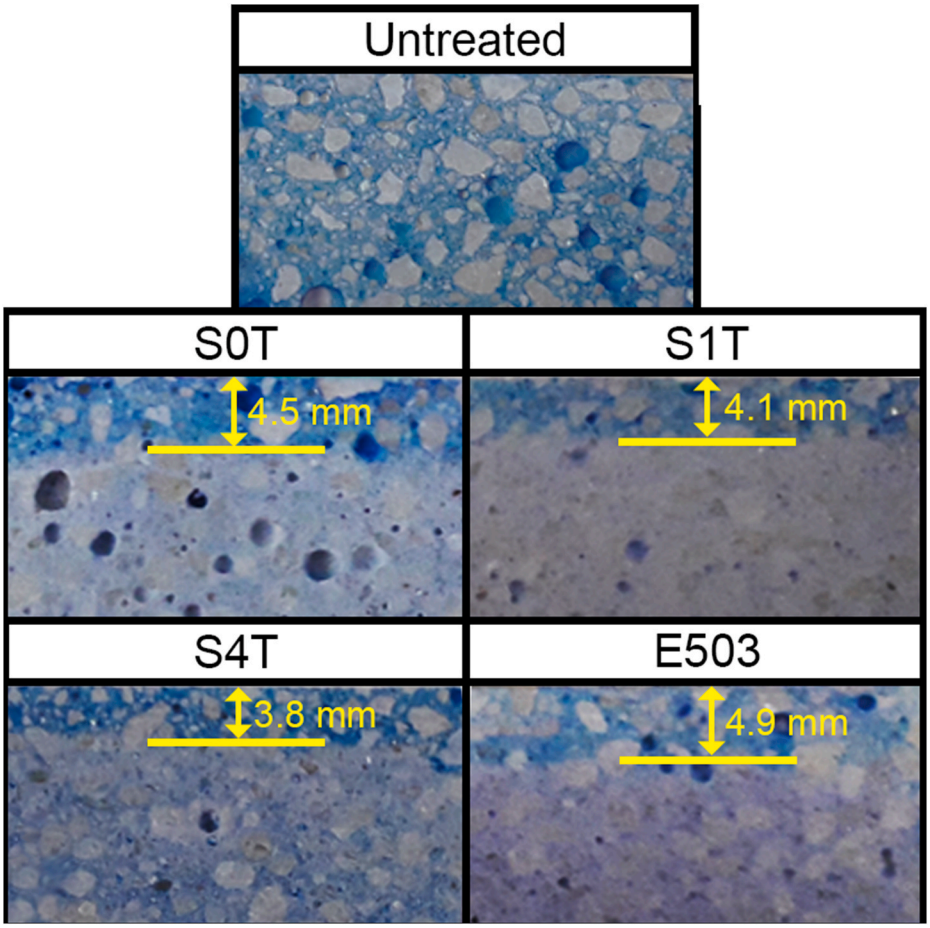

Fig. 4. Images of MB-stained cross sections of the samples in this study.

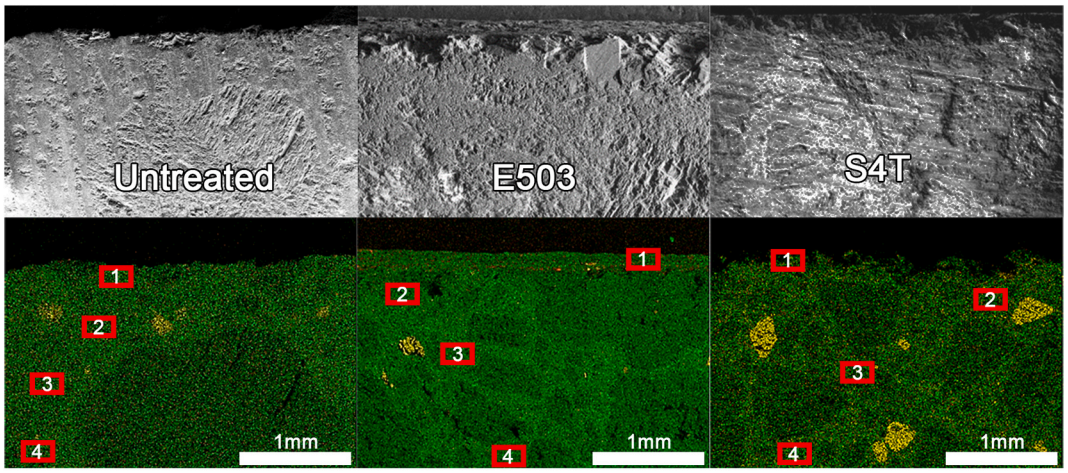

Sample	Atomic %	Area 1	Area 2	Area 3	Area 4
Untreated	Si	8.4	6.1	6.6	9.9
	Ca	88.4	89.4	89.9	87.5
	Ti	3.2	4.5	3.5	2.6
E503	Si	17.8	15.6	15.1	11.1
	Ca	67.7	82.5	83.3	87.5
	Ti	14.5	1.9	1.6	1.4
S4T	Si	17.1	11.5	12.5	17.1
	Ca	69	85.3	86.2	78.7
	Ti	13.9	3.2	1.3	4.2

Fig. 5. SEM images of the samples cross sections, their corresponding XEDS maps showing Ca (green), Si (yellow) and Ti (red) contents and element composition of the numbered areas. (For interpretation of the references to colour in this figure legend, the reader is referred to the Web version of this article.)

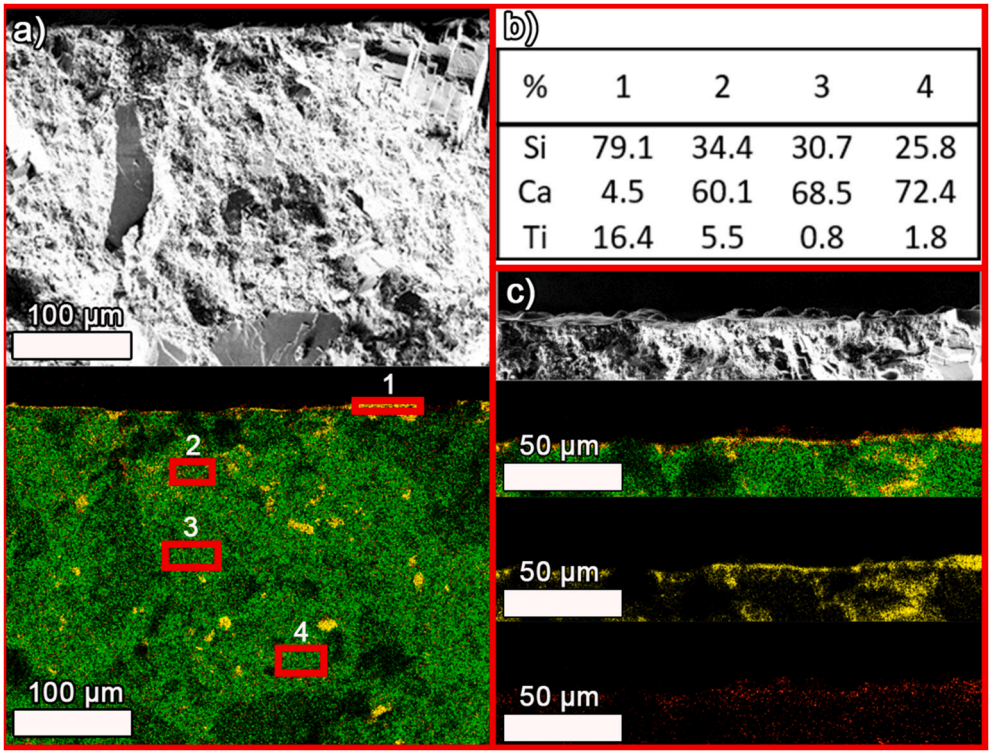

%	1	2	3	4
Si	79.1	34.4	30.7	25.8
Ca	4.5	60.1	68.5	72.4
Ti	16.4	5.5	0.8	1.8

Fig. 6. **a)** SEM image of an S4T sample cross section and its corresponding XEDS map showing Ca (green), Si (yellow) and Ti (red) contents, **b)** element composition of the numbered areas in the "a)" image above, **c)** detail of SEM image of the S4T sample cross section and its corresponding XEDS maps showing Ca (green), Si (yellow) and Ti (red) contents. (For interpretation of the references to colour in this figure legend, the reader is referred to the Web version of this article.)

determined that the atomic Ti/Si ratio was 0.21, which is three times the theoretical Ti/Si ratio of the originally synthesized xerogel before its application. This suggests that the TiO_2 particles accumulate on the substrate surface, as previously observed in the SEM images of the sample surface and that a number of TiO_2 agglomerates do not penetrate the structure but remain on the outside layers of the TiO_2/SiO_2 coating. On the other hand, Ti/Si concentration inside the substrate goes down to 0.16 at just 50 μm deep and then falls drastically to 0.03 at 130 μm. Similarly, Si/Ca ratio also decreases gradually with depth. We could, therefore, conclude that the treatment product can actually penetrate the substrate, but the TiO_2 particles accumulate in the first micrometres inside the sample section, with most of them remaining on the coating surface.

The self-cleaning and air depolluting ability of the treated samples were determined as a function of the reduction of MB, soot, and NO. It should be noted that soot is a key test to evaluate the self-cleaning properties of coatings on concrete-based building materials. Fig. 7 illustrates the degradation through time of both MB and soot under artificial solar light irradiation. The amount of MB removed was calculated using Kubelka-Munk at a given time/Kubelka-Munk at time 0 (KM/KM_0). It could be clearly observed that the highest photoactivity was exhibited by the coatings that contained TiO_2. The amount of MB that was actually removed by S0T and by the untreated sample was attributable to photolysis and to the intrinsic susceptibility of MB to solar light (Fig. 7a). In the particular case of sample S0T, this photolysis phenomenon was promoted by the poorer penetration of MB into the pore structure of the substrate due to the considerable penetration of the silica into the same. Hence, a greater exposure to light radiation promoted a faster degradation.

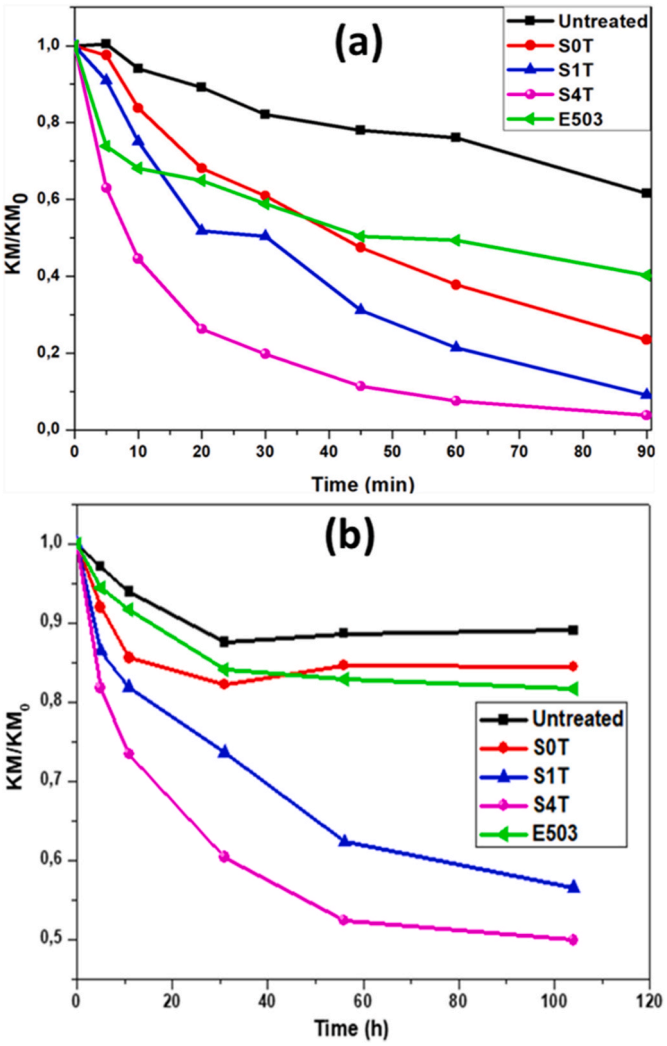

Fig. 7. Evolution of methylene blue (MB) and soot photodegradation, (a) and (b) respectively. (For interpretation of the references to colour in this figure legend, the reader is referred to the Web version of this article.)

The efficiency of the photocatalysts was significantly increased by incorporating TiO_2 NPs to the silica matrix. Additionally, the greater the TiO_2 content the more notable the photocatalytic efficiency of the treatments, so that the amount of MB degraded by samples S1T and S4T was up to 79% and 95%, respectively, in the first 60 min of irradiation. These results are in agreement with the conclusions reached through the observation of the SEM images (Fig. 3), where coatings S1T and S4T showed a highly porous surface with greater surface area that promoted the adsorption of the stain and, therefore, enhanced the photocatalytic activity.

In comparison, the sample that had been treated with the commercial product E503 initially showed a higher rate of degradation, which sharply decreased after the first 10 min of irradiation. On the other hand, at the end of the test, its effectiveness decreased to levels below that exhibited by the sample treated with S0T (TiO_2-free coating). This behaviour can be attributed to the fact that MB can penetrate into the sample through this coating, therefore, the dye that remained on the surface of the coating was easily removed, while the dye that had penetrated the coating degraded more slowly.

Fig. S4 shows the colour evolution of the MB-stained samples, where it can be clearly observed that the stain on the untreated sample was barely altered, while the stains on the treated samples gradually disappeared with irradiation time. Sample S4T, in particular, showed a totally bleached surface after 60 min of irradiation. These results corroborate the findings that have been discussed in the previous section.

The self-cleaning efficiency of the photocatalysts under study was evaluated based on the degradation of soot, as a real staining agent of building materials in urban areas, where a thin layer of black carbon deposits on the surfaces of the substrate, while light penetration is enabled. The corresponding results are presented in Fig. 7b. These results clearly reveal that the degradation trend is similar to that corresponding to MB degradation, but the degradation rate is lower due to soot's greater stability. The obtained results indicate the ability of the studied coatings to eliminate soot from concrete surfaces. Previous studies had confirmed the effectiveness of TiO_2 coatings for soot oxidation [58,59]. It has also been observed that about 10% and 15% of soot would be reduced by either untreated or TiO_2-free coated samples (S0T), respectively, after 104 h of UV–vis irradiation. This might be explained by soot transformations related to aggressive irradiating conditions, temperature or humidity and/or to the mechanical removal produced by the air stream inside the chamber. With respect to the coatings containing TiO_2 photocatalyst, soot elimination efficiency was enhanced by increasing TiO_2 loadings. Thus, the highest efficiency corresponded to the S4T sample, with 50% soot removal after 104 h of irradiation, while S1T would reach 42% removal levels under the same conditions. These results confirm the self-cleaning behaviour of the coatings in the study, as they agree with those previously obtained with regard to MB degradation. Regarding the commercial product E503, it can be seen that this coating did not show any soot removal efficiency, as the amount of soot removed was less than 20% after 104 h of irradiation, which is practically similar to that observed by the untreated sample and by S0T.

The depolluting efficacy of the studied coatings was evaluated as a function of NO reduction, which is a common air pollutant in urban areas. The amounts of NO reduced are listed in Table 2. First, an evident NO conversion of 25% was exhibited by the untreated sample, even if it does not contain any photoactive component. This fact may be attributable to the oxidation of NO to NO_2 supported by the stationary conditions of the test, and the subsequent removal of NOx by reaction with

the portlandite present in concrete, that produces calcium nitrates and nitrites. Despite this, it is clear that the presence of TiO_2 significantly increased NO conversion, which confirms its photocatalytic properties. S1T and E503 coatings showed a slight enhancement of their NO photocatalytic conversion efficiency when compared to the untreated samples, with 38% and 35% conversions achieved by S1T and E503, respectively. Sample S4T, on the other hand, nearly doubled the conversion of the untreated sample, with a total NO conversion of 49%. These results corroborate that the S4T product is a promising and effective treatment to eliminate from the building materials the atmospheric NO_x that is present in urban areas.

With the aim of evaluating the hydrophilicity changes of the treated samples, the Water Contact Angle (WCA) on concrete substrates kept in the absence of light and then exposed to UV–vis light was determined. Note that 10 measurements were taken of each sample and the average value was registered. The obtained WCA values are presented in Table 2. Before they were exposed to the light, all the treated samples exhibited somewhat higher WCA than the untreated samples, except for those that were treated with E503 and whose WCA remained similar to that of the untreated samples. This higher WCA could be due to the coatings filling up the entire porous structure of the concrete samples. Furthermore, due to the hydrophilic character of TiO_2, WCA values slightly decreased as TiO_2 content was increased [60]. After the samples were activated by exposing them to UV–Vis, no significant differences could be observed with regard to WCA in S0T, E503 and the untreated samples. In contrast, the samples that had been treated with the TiO_2 NP-containing coatings exhibited higher hydrophilic properties that resulted in a drop of their WCA value. This effect was particularly significant on the S4T sample because of its greater TiO_2 loading, which clearly suggests that the addition of TiO_2 to the coatings promotes photo-induced hydrophilicity.

3.3. Durability

Good adhesion and a long durability are key factors for efficient outdoor photocatalytic coating applications. For this reason, a number of peeling tests were conducted to verify that a satisfactory adherence of the coatings onto the substrates was achieved. The weight losses of the untreated samples and their treated counterparts are listed in Table 2. It is clear that the developed treatments have considerably reduced the amount of material removed from the samples' surfaces, being their values practically zero. These results indicate that the coatings adhered well onto the substrates and achieve an effective consolidation of the concrete surface. Regarding the samples treated with the commercial product, the material removed was three times the amount corresponding to the untreated samples. Therefore, the coatings produced by the commercial product have exhibited a poor adhesion on concrete substrates. In order to confirm that the removed material corresponded to the coating, the material that had got stuck onto the tape was analysed by SEM (see Fig. S5 in the Supplementary Material). The EDS map and elementary analysis clearly indicate the presence of TiO_2 NPs among the materials removed, which confirms that TiO_2 had been detached and, consequently, the treatment durability would be diminished. The loss of material from sample E503 could be due to the presence of cracks on the coating surface or it could also be associated to the intrinsic nature of the product, which consists in nanoparticles dispersed in solvent.

The coatings' durability was also assessed through triplicate MB degradation cycle tests. The samples employed in this study were S0T, S1T and S4T as well as an untreated sample for comparison purposes. The tests were conducted as described in the previous sections. After each test, the samples were irradiated (in a solar degradation chamber) for 24 h in order to thoroughly remove the rest of the dye that might remain on their surfaces. The obtained results are displayed in Fig. 8. All the coatings exhibited similar behaviours during the three photocatalytic degradation cycles, where the amount of MB removed slightly

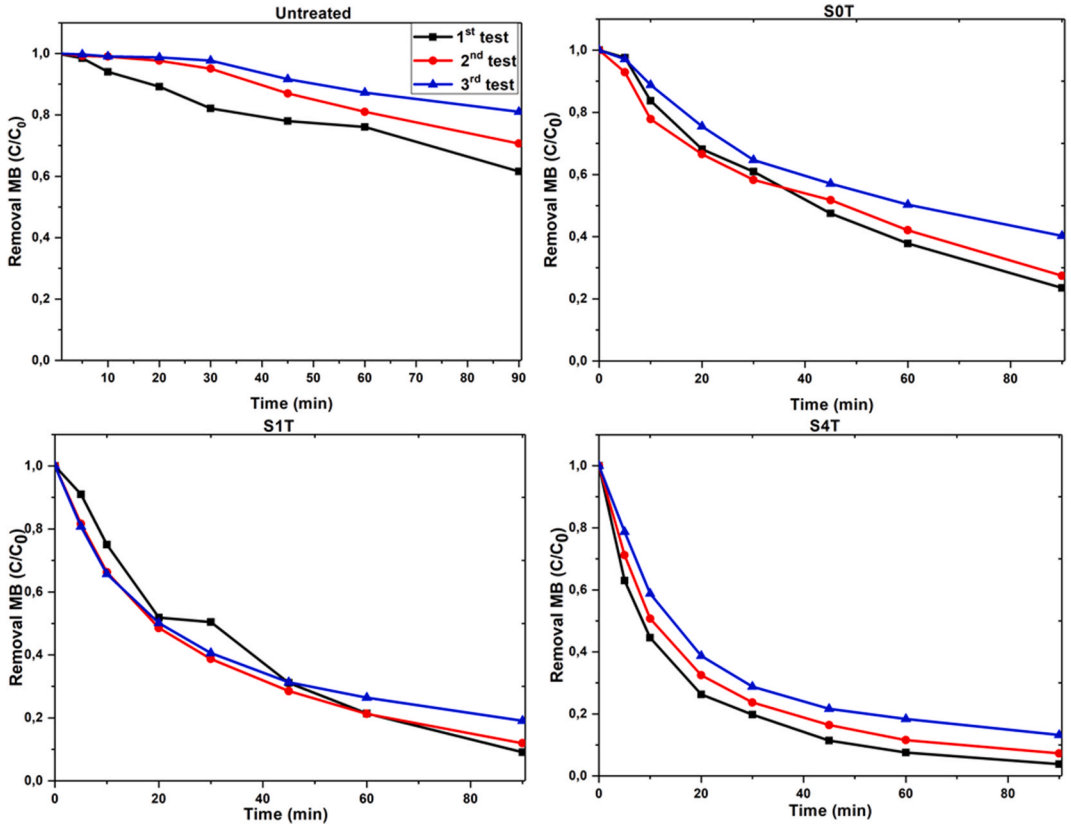

Fig. 8. Results of MB degradation repeatability cycles.

decreased with each cycle. Since a similar decrease in MB removal was observed in the untreated sample, we could conclude this drop is not related to the efficiency of the photocatalysts, but rather to the amount of MB accumulated in the pores of the concrete substrates. These results corroborate the high stability of the photocatalytic coatings, since they continue to exhibit self-cleaning behaviour after prolonged exposure to UV–Vis light.

Finally, the durability of the self-cleaning coatings was evaluated in real-life conditions, so that the effect of exposure to real-life conditions on their self-cleaning effectiveness could be determined. The samples were positioned at a site where they were exposed to a wide range of contaminants (Seville city centre) for four months. When their exposure period was completed the samples were brought into the lab and their self-cleaning durability was determined based on MB photodegradation. Before running the self-cleaning tests, all the dust deposited on the samples' surfaces was removed by means of a pressured air jet and water. Fig. 9 illustrates the evolution of MB photodegradation before and after exposure to real-life conditions. It was obvious that the samples had preserved their self-cleaning properties regardless of the external conditions they had been exposed to, since they exhibited a high MB photodegradation efficiency. In addition, their degradation trend was similar to the one they presented before being exposed to real-life conditions. Nevertheless, by comparing the photodegradation efficiency before and after exposure (Fig. 9b), it could be clearly seen that the coatings had experienced a slight decrease in their photocatalytic efficiency. This decrease was as high as 30% in S0T and S1T samples, while sample S4T exhibited just a slight decrease of only 8%, which again corroborates that S4T is the most suitable treatment for building materials because of its superior performance and durability. This finding broadly supports the conclusions reported by other studies, where different methods were employed to investigate the durability of TiO_2 self-cleaning coatings under indoor and outdoor conditions [20,61–63]. The results from these studies revealed that TiO_2 coatings retained their self-cleaning properties regardless of the elapsed time.

In order to verify the previous findings, SEM was employed to determine if the topography of the samples' surfaces had undergone any changes as a result of their exposure to outdoor conditions. The SEM images of the studied samples, before and after exposure to real-life condition, are presented in Fig. 10. Some obvious differences can be observed in the samples that had been subjected to outdoor conditions. The results indicate that coating S0T was partially removed after the durability test, which had allowed MB to penetrate the substrate. Regarding the TiO_2 containing samples, it can be clearly seen that the coatings most superficial layer had been swept away and turned into practically smooth surfaces due to a number of factors. When the photocatalytic coatings were compared, it could be observed that S4T remained as the most particulate surface, which indicates that it still contained the largest loading of TiO_2 particles, which in turn means a better preservation of its photocatalytic properties. These results explain the long self-cleaning durability of the studied coatings.

4. Conclusions

In summary, this paper has investigated the self-cleaning and air depolluting properties of TiO_2/SiO_2 coatings applied onto concrete substrates. Different concentrations of TiO_2 NPs were added to the coating product to verify any possible variations in their photocatalytic activity. A commercial product, known as E503, was also employed for comparison purposes.

When the different products were applied, they generated homogeneous layers on the concrete substrates, with particulate surfaces that indicated the presence of TiO_2 NPs on their uppermost superficial layers. In addition, the experimental coatings exhibited crack-free surfaces, unlike the coating generated by the commercial product E503, where cracks could be observed. The efficacy of these coatings was determined according to their capacity to degrade two substances, MB and soot, and their air de-polluting ability was evaluated by measuring NO oxidation. It was corroborated that the coatings' photocatalytic efficiency increased as the sols' concentration of TiO_2 NPs was increased. Therefore, the greater the TiO_2 loading, the highest efficiency was exhibited by the coatings.

Two methods have been used to determine self-cleaning durability. First, by running MB degradation tests on the samples in triplicate. According to the results obtained the coatings present long-term self-cleaning properties, with a very slight drop in their photocatalytic efficiency. Then, the samples were placed outdoor and exposed to a wide range of environmental pollutants for a period of four months. Subsequently, their self-cleaning effectiveness was determined as a function of MB degradation. According to our results, the coatings maintained their MB degradation trends and their photocatalytic efficiency went down by just a slightly margin, while S4T (the sol with the highest TiO_2 NPs loading) presented the slightest efficiency loss. The SEM images of the samples after outdoor exposure allowed to confirm that the coatings were still covering the substrates and presented similar self-cleaning efficiency levels as before being exposed to outdoor conditions.

CRediT authorship contribution statement

M.L. Almoraima Gil: Investigation, Writing – original draft, Writing – review & editing.

Declaration of competing interest

The authors declare that they have no known competing financial

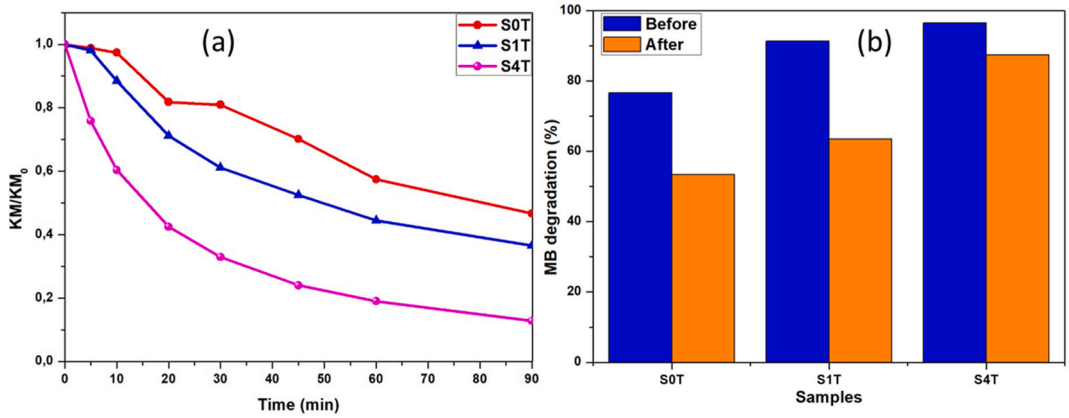

Fig. 9. Evolution of MB photodegradation: (a) after 4 months under outdoor conditions and (b) comparison of total amount of MB removed before and after the exposure to real-life conditions.

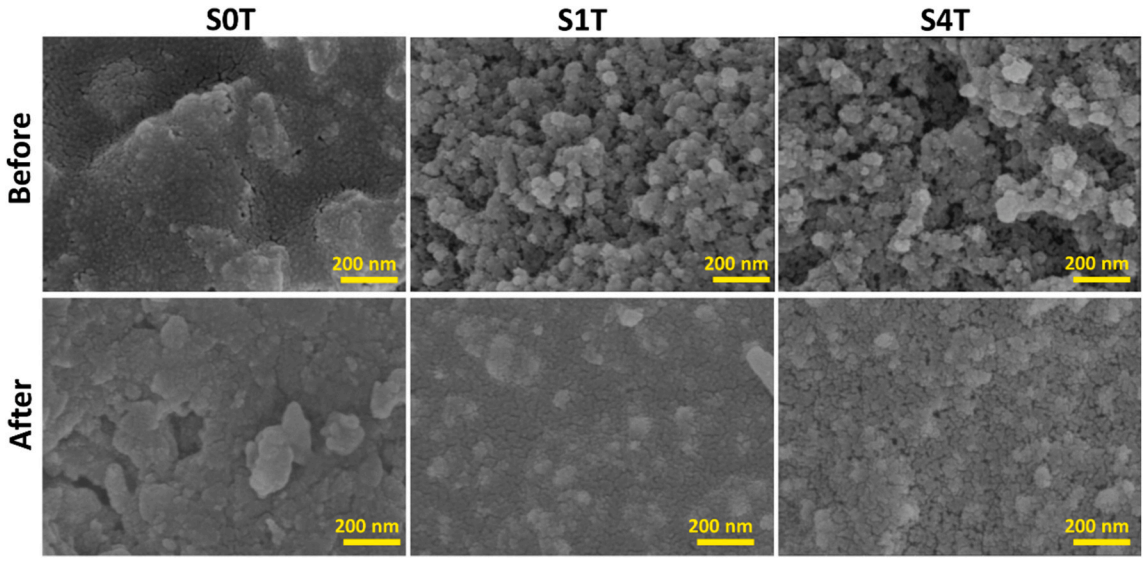

Fig. 10. SEM images of treated concrete surfaces before and after 4 months of exposure to real-life conditions.

interests or personal relationships that could have appeared to influence the work reported in this paper.

Acknowledgements

This work has been supported by the Spanish Government MAT2017-84228-R (MINECO/AEI//FEDER, UE) and PID2020-115843RB-I00/AEI/10.13039/501100011033. This work has been co-financed by the European Union under the 2014–2020 ERDF Operational Programme and by the Department of Economic Transformation, Industry, Knowledge, and Universities of the Regional Government of Andalusia. Project reference: FEDER-UCA18-106613.

Appendix A. Supplementary data

Supplementary data to this article can be found online at https://doi.org/10.1016/j.buildenv.2021.108743.

References

[1] European Environment Agency, European Union Emission Inventory Report 1990–2014 under the UNECE Convention on Long-Range Transboundary Air Pollution, LRTAP, 2014.
[2] L. Bauleo, S. Bucci, C. Antonucci, R. Sozzi, M. Davoli, F. Forastiere, C. Ancona, Long-term exposure to air pollutants from multiple sources and mortality in an industrial area: a cohort study, Occup. Environ. Med. 76 (2019) 48–57, https://doi.org/10.1136/oemed-2018-105059.
[3] F.J. Kelly, J.C. Fussell, Size, source and chemical composition as determinants of toxicity attributable to ambient particulate matter, Atmos. Environ. 60 (2012) 504–526, https://doi.org/10.1016/j.atmosenv.2012.06.039.
[4] ICOMOS, ISCS, Illustrated glossary on stone deterioration patterns. http://www.icomos.org/publications/monuments_and_sites/15/pdf/Monuments_and_Sites_15_ISCS_Glossary_Stone.pdf, 2008.
[5] WHO, Health relevance of particulate matter from various sources, Beilstein J. Nanotechnol. 5 (2007) 1590–1602.
[6] M. Gallus, V. Akylas, F. Barmpas, A. Beeldens, E. Boonen, A. Boréave, M. Cazaunau, H. Chen, V. Daële, J.F. Doussin, Y. Dupart, C. Gaimoz, C. George, B. Grosselin, H. Herrmann, S. Ifang, R. Kurtenbach, M. Maille, A. Mellouki, K. Miet, F. Mothes, N. Moussiopoulos, L. Poulain, R. Rabe, P. Zapf, J. Kleffmann, Photocatalytic de-pollution in the Leopold II tunnel in Brussels: NOx abatement results, Build, Environ. Times 84 (2015) 125–133, https://doi.org/10.1016/j.buildenv.2014.10.032.
[7] T. Martinez, A. Bertron, E. Ringot, G. Escadeillas, Degradation of NO using photocatalytic coatings applied to different substrates, Build. Environ. 46 (2011) 1808–1816, https://doi.org/10.1016/j.buildenv.2011.03.001.
[8] X. Tang, L. Ughetta, S.K. Shannon, S. Houzé de l'Aulnoit, S. Chen, R.A.T. Gould, M. L. Russell, J. Zhang, G. Ban-Weiss, R.L.A. Everman, F.W. Klink, R. Levinson, H. Destaillats, De-pollution efficacy of photocatalytic roofing granules, Build. Environ. 160 (2019) 106058, https://doi.org/10.1016/j.buildenv.2019.03.056.
[9] E.A. Shchelokova, V.V. Tyukavkina, A.V. Tsyryatyeva, A.G. Kasikov, Synthesis and characterization of SiO2-TiO2 nanoparticles and their effect on the strength of self-cleaning cement composites, Construct. Build. Mater. 283 (2021) 122769, https://doi.org/10.1016/j.conbuildmat.2021.122769.
[10] A. Fujishima, K. Honda, Electrochemical photolysis of water at a semiconductor electrode, Nature 238 (1972) 37–38, https://doi.org/10.1038/238037a0.
[11] H. Zangeneh, A.A.L. Zinatizadeh, M. Habibi, M. Akia, M. Hasnain Isa, Photocatalytic oxidation of organic dyes and pollutants in wastewater using different modified titanium dioxides: a comparative review, J. Ind. Eng. Chem. 26 (2015) 1–36, https://doi.org/10.1016/j.jiec.2014.10.043.
[12] M.H. Habibi, S. Tangestaninejad, B. Yadollahi, Photocatalytic mineralisation of mercaptans as environmental pollutants in aquatic system using TiO2suspension, Appl. Catal. B Environ. 33 (2001) 57–63, https://doi.org/10.1016/S0926-3373(01)00158-8.
[13] D.G. Shchukin, D.V. Sviridov, Photocatalytic processes in spatially confined micro- and nanoreactors, J. Photochem. Photobiol. C Photochem. Rev. 7 (2006) 23–39, https://doi.org/10.1016/j.jphotochemrev.2006.03.002.
[14] R. Zhang, L. Gao, Q. Zhang, Photodegradation of surfactants on the nanosized TiO2prepared by hydrolysis of the alkoxide titanium, Chemosphere 54 (2004) 405–411, https://doi.org/10.1016/S0045-6535(03)00588-5.
[15] S.D. Richardson, A.D. Thruston, T.W. Collette, K.S. Patterson, B.W. Lykins, J. C. Ireland, Identification of Tio2/UV disinfection byproducts in drinking water, Environ. Sci. Technol. 30 (1996) 3327–3334, https://doi.org/10.1021/es960142m.
[16] P.S. Awati, S.V. Awate, P.P. Shah, V. Ramaswamy, Photocatalytic decomposition of methylene blue using nanocrystalline anatase titania prepared by ultrasonic technique, Catal. Commun. 4 (2003) 393–400, https://doi.org/10.1016/S1566-7367(03)00092-X.
[17] D. Beydoun, R. Amal, G. Low, S. McEvoy, Role of nanoparticles in photocatalysis, J. Nanoparticle Res. 1 (1999) 439–458, https://doi.org/10.1023/A:1010044830871.
[18] M.R. Prairie, L.R. Evans, B.M. Stange, S.L. Martinez, An investigation of titanium dioxide photocatalysis for the treatment of water contaminated with metals and organic chemicals, Environ. Sci. Technol. 27 (1993) 1776–1782, https://doi.org/10.1021/es00046a003.
[19] P. Cheng, C. Deng, M. Gu, X. Dai, Effect of urea on the photoactivity of titania powder prepared by sol-gel method, Mater. Chem. Phys. 107 (2008) 77–81, https://doi.org/10.1016/j.matchemphys.2007.06.051.
[20] L. Graziani, E. Quagliarini, F. Bondioli, M. D'Orazio, Durability of self-cleaning TiO2 coatings on fired clay brick façades: effects of UV exposure and wet & dry cycles, Build. Environ. 71 (2014) 193–203, https://doi.org/10.1016/j.buildenv.2013.10.005.
[21] R. Wang, K. Hashimoto, A. Fujishima, Light-induced amphiphilic surfaces, Nature 388 (1997) 431–432, https://doi.org/10.1038/41233.
[22] A. Fujishima, X. Zhang, D.A. Tryk, TiO2 photocatalysis and related surface phenomena, Surf. Sci. Rep. 63 (2008) 515–582, https://doi.org/10.1016/j.surfrep.2008.10.001.
[23] A. Fujishima, T.N. Rao, D.A. Tryk, Titanium dioxide photocatalysis, J. Photochem. Photobiol. C Photochem. Rev. 1 (2000) 1–21, https://doi.org/10.1016/S1389-5567(00)00002-2.
[24] Q. Jiang, C. Ding, Y. Liu, A type of novel glass for indoor air cleaning under visible-light, Build, Environ. Times 137 (2018) 226–234, https://doi.org/10.1016/j.buildenv.2018.04.013.
[25] W. Xie, M. Zhang, D. Liu, W. Lei, L. Sun, X. Wang, J. Accepted, Reactive Yellow161 decolorization by TiO 2/porous BNNSs composites in cotton dyeing effluent. https://doi.org/10.1021/acssuschemeng.6b01896, 2016.

[26] M. Kim, H. Jung, E. Park, J. Jurng, Performance of an air purifier using a MnOx/TiO2 catalyst-coated filter for the decomposition of aldehydes, VOCs and ozone: an experimental study in an actual smoking room, Build. Environ. 186 (2020) 107247, https://doi.org/10.1016/j.buildenv.2020.107247.
[27] S. Veltri, A.M. Palermo, G. De Filpo, F. Xu, Subsurface treatment of TiO 2 nanoparticles for limestone: prolonged surface photocatalytic biocidal activities, Build. Environ. 149 (2019) 655–661, https://doi.org/10.1016/j.buildenv.2018.10.038.
[28] I. Alfieri, A. Lorenzi, L. Ranzenigo, L. Lazzarini, G. Predieri, P.P. Lottici, Synthesis and characterization of photocatalytic hydrophobic hybrid TiO2-SiO2 coatings for building applications, Build, Environ. Times 111 (2017) 72–79, https://doi.org/10.1016/j.buildenv.2016.10.019.
[29] L. Pinho, M.J. Mosquera, Titania-silica nanocomposite photocatalysts with application in stone self-cleaning, J. Phys. Chem. C 115 (2011) 22851–22862, https://doi.org/10.1021/jp2074623.
[30] J.S. Pozo-Antonio, A. Dionísio, Self-cleaning property of mortars with TiO2addition using real diesel exhaust soot, J. Clean. Prod. 161 (2017) 850–859, https://doi.org/10.1016/j.jclepro.2017.05.202.
[31] A. Folli, S.B. Campbell, J.A. Anderson, D.E. MacPhee, Role of TiO2surface hydration on NO oxidation photo-activity, J. Photochem. Photobiol. Chem. 220 (2011) 85–93, https://doi.org/10.1016/j.jphotochem.2011.03.017.
[32] M. Horgnies, I. Dubois-Brugger, E.M. Gartner, NO x de-pollution by hardened concrete and the influence of activated charcoal additions, Cement Concr. Res. 42 (2012) 1348–1355, https://doi.org/10.1016/j.cemconres.2012.06.007.
[33] M. Smits, C. kit Chan, T. Tytgat, B. Craeye, N. Costarramone, S. Lacombe, S. Lenaerts, Photocatalytic degradation of soot deposition: self-cleaning effect on titanium dioxide coated cementitious materials, Chem. Eng. J. 222 (2013) 411–418, https://doi.org/10.1016/j.cej.2013.02.089.
[34] R. Zouzelka, J. Rathousky, Photocatalytic abatement of NOx pollutants in the air using commercial functional coating with porous morphology, Appl. Catal. B Environ. 217 (2017) 466–476, https://doi.org/10.1016/j.apcatb.2017.06.009.
[35] C. Mendoza, A. Valle, M. Castellote, A. Bahamonde, M. Faraldos, TiO2 and TiO2-SiO2 coated cement: comparison of mechanic and photocatalytic properties, Appl. Catal. B Environ. 178 (2015) 155–164, https://doi.org/10.1016/j.apcatb.2014.09.079.
[36] M.M. Ballari, M. Hunger, G. Hüsken, H.J.H. Brouwers, NOxphotocatalytic degradation employing concrete pavement containing titanium dioxide, Appl. Catal. B Environ. 95 (2010) 245–254, https://doi.org/10.1016/j.apcatb.2010.01.002.
[37] J. MacMullen, J. Radulovic, Z. Zhang, H.N. Dhakal, L. Daniels, J. Elford, M. A. Leost, N. Bennett, Masonry remediation and protection by aqueous silane/siloxane macroemulsions incorporating colloidal titanium dioxide and zinc oxide nanoparticulates: mechanisms, performance and benefits, Construct. Build. Mater. 49 (2013) 93–100, https://doi.org/10.1016/j.conbuildmat.2013.08.019.
[38] C. Mendoza, A. Valle, M. Castellote, A. Bahamonde, M. Faraldos, TiO2 and TiO2-SiO2 coated cement: comparison of mechanic and photocatalytic properties, Appl. Catal. B Environ. 178 (2015) 155–164, https://doi.org/10.1016/j.apcatb.2014.09.079.
[39] D. composite powders deposited on cement-based materials: R.B. removal and the bonding mechanism P. Wang, D. Hou, S. Stephan, L. Huang, P. Zhang, X. Yang, Cheng, SiO2/TiO2 composite powders deposited on cement-based materials: rhodamine B removal and the bonding mechanism, Construct. Build. Mater. 241 (2020) 118124, https://doi.org/10.1016/j.conbuildmat.2020.118124.
[40] C. Kapridaki, L. Pinho, M.J. Mosquera, P. Maravelaki-Kalaitzaki, Producing photoactive, transparent and hydrophobic SiO2-crystalline TiO2 nanocomposites at ambient conditions with application as self-cleaning coatings, Appl. Catal. B Environ. 156–157 (2014) 416–427, https://doi.org/10.1016/j.apcatb.2014.03.042.
[41] L. Pinho, F. Elhaddad, D.S. Facio, M.J. Mosquera, A novel TiO2-SiO2 nanocomposite converts a very friable stone into a self-cleaning building material, Appl. Surf. Sci. 275 (2013) 389–396, https://doi.org/10.1016/j.apsusc.2012.10.142.
[42] A. Rosales, A. Maury-Ramírez, R.M.-D. Gutiérrez, C. Guzmán, K. Esquivel, SiO2@TiO2 coating: synthesis, physical characterization and photocatalytic evaluation, Coatings 8 (2018) 120, https://doi.org/10.3390/coatings8040120.
[43] Natural stone test methods. Determination of real density and apparent density, and of total and open porosity, Eur. Stand. (2006) 10. https://www.sis.se/en/produkter/mining-and-minerals/mining-and-quarrying/ssen19362006/.
[44] M. Thommes, B. Smarsly, M. Groenewolt, P.I. Ravikovitch, A.V. Neimark, Adsorption hysteresis of nitrogen and argon in pore networks and characterization of novel micro- and mesoporous silicas, Langmuir 22 (2006) 756–764, https://doi.org/10.1021/la051686h.
[45] R.S. Berns, Billmeyer and Saltzman 's Principles of Color Technology, third ed., Wiley-Interscience, New York, 2000.
[46] M. Drdácký, J. Lesák, S. Rescic, Z. Slížková, P. Tiano, J. Valach, Standardization of peeling tests for assessing the cohesion and consolidation characteristics of historic stone surfaces, Mater. Struct. 45 (2012) 505–520, https://doi.org/10.1617/s11527-011-9778-x.
[47] ISO 10678: 2010, Fine Ceramics, Advanced Technical Ceramics Determination of Photocatalytic Activity of Surfaces in an Aqueous Medium by Degradation of Methylene Blue, International Organization for Standardization, Geneva, Switzerland, 2010.
[48] M. Luna, J. Delgado, M. Gil, M. Mosquera, TiO2-SiO2 coatings with a low content of AuNPs for producing self-cleaning building materials, Nanomaterials 8 (2018) 177, https://doi.org/10.3390/nano8030177.
[49] M. Luna, M.J. Mosquera, H. Vidal, J.M. Gatica, Au-TiO_2/SiO_2 photocatalysts for building materials: self-cleaning and de-polluting performance, Build, Environ. Times 164 (2019) 106347, https://doi.org/10.1016/j.buildenv.2019.106347.
[50] M.A. Ceballos, La calidad del aire en el Estado español durante 2018, Medi Ambient Tecnol. i Cult, 4, https://www.ecologistasenaccion.org/?p=96516, 2018.
[51] L. Pinho, M.J. Mosquera, Photocatalytic activity of TiO2–SiO2 nanocomposites applied to buildings: influence of particle size and loading, Appl. Catal. B Environ. 134–135 (2013) 205–221, https://doi.org/10.1016/j.apcatb.2013.01.021.
[52] P. Wilhelm, D. Stephan, On-line tracking of the coating of nanoscaled silica with titania nanoparticles via zeta-potential measurements, J. Colloid Interface Sci. 293 (2006) 88–92, https://doi.org/10.1016/j.jcis.2005.06.047.
[53] M. Luna, J.M. Gatica, H. Vidal, M.J. Mosquera, Au-TiO_2/SiO_2 photocatalysts with NO_x depolluting activity: influence of gold particle size and loading, Chem. Eng. J. 368 (2019), https://doi.org/10.1016/j.cej.2019.02.167.
[54] M. Thommes, K. Kaneko, A.V. Neimark, J.P. Olivier, F. Rodriguez-Reinoso, J. Rouquerol, K.S.W. Sing, Physisorption of gases, with special reference to the evaluation of surface area and pore size distribution (IUPAC Technical Report), Pure Appl. Chem. 87 (2015) 1051–1069, https://doi.org/10.1515/pac-2014-1117.
[55] M. Kruk, M. Jaroniec, Gas adsorption characterization of ordered organic-inorganic nanocomposite materials, Chem. Mater. 13 (2001) 3169–3183, https://doi.org/10.1021/cm0101069.
[56] J.D. Rodrigues, A. Grossi, Indicators and ratings for the compatibility assessment of conservation actions, J. Cult. Herit. 8 (2007) 32–43, https://doi.org/10.1016/j.culher.2006.04.007.
[57] L. Pinho, J.C. Hernández-Garrido, J.J. Calvino, M.J. Mosquera, 2D and 3D characterization of a surfactant-synthesized TiO2–SiO2 mesoporous photocatalyst obtained at ambient temperature, Phys. Chem. Chem. Phys. 15 (2013) 2800, https://doi.org/10.1039/c2cp42606d.
[58] M.C. Lee, W. Choi, Solid phase photocatalytic reaction on the Soot/TiO2 interface: the role of migrating OH radicals, J. Phys. Chem. B 106 (2002) 11818–11822, https://doi.org/10.1021/jp026617f.
[59] M. Luna, M.J. Mosquera, H. Vidal, J.M. Gatica, Au-TiO2/SiO2 photocatalysts for building materials: self-cleaning and de-polluting performance, Build. Environ. 164 (2019), https://doi.org/10.1016/j.buildenv.2019.106347.
[60] G. Soliveri, V. Sabatini, H. Farina, M.A. Ortenzi, D. Meroni, A. Colombo, Double side self-cleaning polymeric materials: the hydrophobic and photoactive approach, Colloids Surf. A Physicochem. Eng. Asp. 483 (2015) 285–291, https://doi.org/10.1016/j.colsurfa.2015.06.059.
[61] E.I. Cedillo-González, V. Barbieri, P. Falcaro, L.M. Torres-Martínez, I. Juárez-Ramírez, L. Villanova, M. Montecchi, L. Pasquali, C. Siligardi, Influence of domestic and environmental weathering in the self-cleaning performance and durability of TiO 2 photocatalytic coatings, Build, Environ. Times 132 (2018) 96–103, https://doi.org/10.1016/j.buildenv.2018.01.028.
[62] P.M. Carmona-Quiroga, S. Martínez-Ramírez, H.A. Viles, Efficiency and durability of a self-cleaning coating on concrete and stones under both natural and artificial ageing trials, Appl. Surf. Sci. 433 (2018) 312–320, https://doi.org/10.1016/j.apsusc.2017.10.052.
[63] A. Calia, M. Lettieri, M. Masieri, Durability assessment of nanostructured TiO2coatings applied on limestones to enhance building surface with self-cleaning ability, Build. Environ. 110 (2016) 1–10, https://doi.org/10.1016/j.buildenv.2016.09.030.